Dendritic Ni-P-Coated Melamine Foam for a Lightweight, Low-Cost, and Amphipathic Three-Dimensional Current Collector for Binder-Free Electrodes

*Xiao-lei Huang, Dan Xu, Shuang Yuan, De-long Ma, Sai Wang, Huai-yu Zheng, and Xin-bo Zhang**

Any future success in the global effort to shift energy usage away from fossil fuels to renewable sources depends on large-scale electrical energy storage, for example using rechargeable batteries, such as lithium ion batteries (LIBs) and sodium ion batteries (SIBs); a significant enhancement in both the energy- and power-density of LIBs and SIBs is therefore a long-standing goal.[1] To this end, the design of new electrode materials with higher capacity to replace those used commercially is an urgent necessity. Unfortunately, the electrical conductivity of most such candidates, including metal oxide or metal fluoride materials, is intrinsically very low. Even worse, as conventional battery electrodes are mainly fabricated based on a planar current collector, even with the help of polymeric binder the electrical contact between electroactive materials and the current collector is still prone to be lost as a result of the serious electrode pulverization caused by the repeated huge volume expansion/shrinkage upon lithium or sodium insertion/extraction.[2] Furthermore, the addition of inactive, insulating, and swellable (in electrolyte) polymeric binders would inevitably impede efforts to increase the capacity and rate capability and to reduce the manufacturing costs of batteries, which is vital for large-scale electric energy storage applications.[3] In order to meet these challenges by building a binder-free electrode, current collectors based on a completely new design of three-dimensional (3D) multifunctional architectures and micrometer-scale roughness that can simultaneously improve the essential reaction interphases for the fundamental energy storage processes, including electronic and ionic conductivity, mass and charge transport, and alleviation of the volume variation, are thus urgently required while still remaining very challenging.[4]

Dr. X.-l. Huang, Dr. D. Xu, S. Yuan, D.-l. Ma, S. Wang, H.-y. Zheng, Prof. X.-b. Zhang
State Key Laboratory of Rare Earth Resource Utilization
Changchun Institute of Applied Chemistry
Chinese Academy of Sciences
Changchun, Jilin 130022, P. R. China
E-mail: xbzhang@ciac.ac.cn
Dr. X.-l. Huang, S. Yuan, D.-l. Ma, S. Wang, H.-y. Zheng
Key Laboratory of Automobile Materials
Ministry of Education and
College of Materials Science and Engineering
Jilin University
Changchun, Jilin 130012, P. R. China

DOI: 10.1002/adma.201402717

Porous metals have been considered as promising candidates for the construction of 3D current collectors because of their high surface area and superior electronic conductivity. Up to now, electrodeposition,[5] de-alloying,[6] and magnetron sputtering/e-beam evaporation[4a,b] are the main methods that have been employed to prepare 3D porous metal current collectors. Unfortunately, all these methods suffer from more or less severe drawbacks, such as requiring special equipment or complicated preparation processes that involve a high-cost template or are energy intensive and time consuming, and thus present difficulties for large-scale fabrication. Even so, the obtained 3D porous metal current collectors are limited to pure metals in the form of a short metal nanowire and/or thin porous metal,[5,6] which are intrinsically high in density and cost, and especially, poor in mechanical strength (no flexibility, easily destroyed during the preparation and long-term running of the batteries). Although 3D porous carbon current collectors are relatively lightweight and flexible,[7] they are unstable for LIB and SIB anodes because of the reaction between lithium or sodium metal and carbon.[8] Furthermore, current 3D current collectors are narrow in electrochemical window and, especially, have a smooth surface, which makes the fabrication of a binder-free electrode impossible as its adhesion with electroactive materials is very poor. Therefore, the development of a new strategy for the scalable fabrication of a lightweight, low-cost, robust 3D current collector with micrometer-scale roughness (dendritic) for use in a wide voltage window (0–5 V) is urgently required.

In this Communication, we report the fabrication of a lightweight, low-cost, and robust 3D porous dendritic current collector (3DDC) that has high electronic conductivity, abundant interconnected ion/electron and mass transport pathways, and superior electrochemical stability over a wide voltage range (0–5 V). Unexpectedly, the obtained 3DDC is dendritic and amphipathic, which intrinsically enables the successful fabrication of a robust binder-free electrode (without the help of an insulating and inactive binder). As a proof-of-concept application, a binder-free 3DDC/GeO_2 electrode has been successfully obtained, which shows superior electrochemical performance even compared to binder-containing counterparts.

Figure 1 shows the synthesis strategy for the 3DDC. First, the catalyst nanoparticles were coated on melamine foam (white) by a chemical strategy. Then, the dendritic metal nickel (dark gray) was deposited on the surface of the melamine foam by means of electroless nickel plating, which is a well-known route for producing commercial nickel foam.

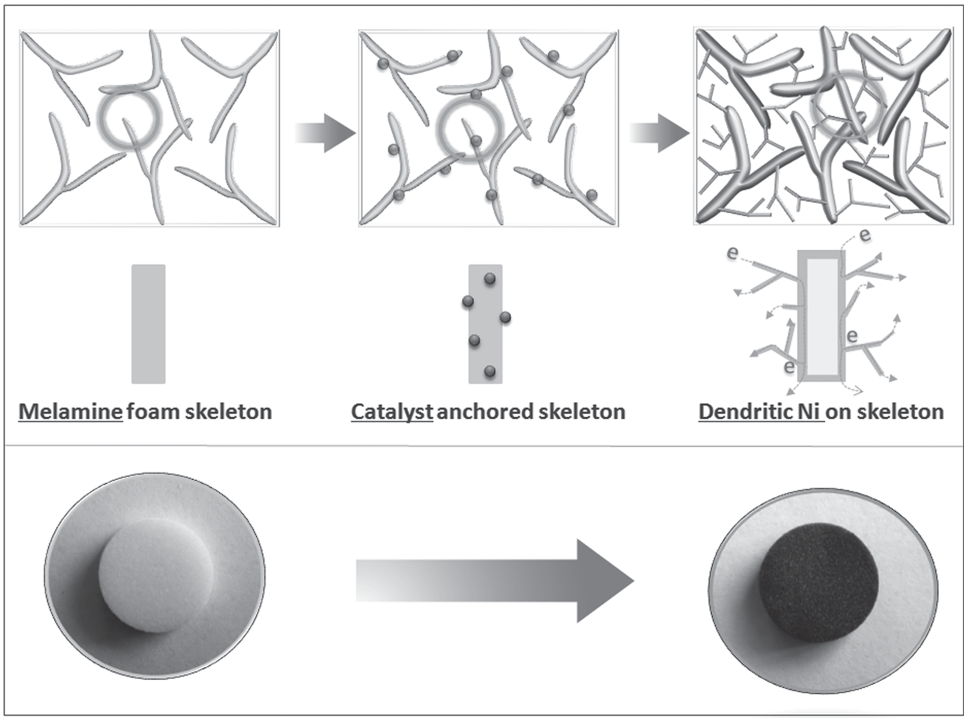

Figure 1. Schematic representation of the fabrication process of the 3DDC.

In order to demonstrate the morphology and structure evolution of the 3DDC, field-emission scanning electron microscopy (FE-SEM) was employed. **Figures 2**a-d show FE-SEM images of the melamine foam and the as-synthesized products. The melamine foam has a porous structure, and the skeleton is ca. 3–4 μm in diameter with a smooth surface (Figure 2a,b). In contrast, the as-synthesized products have a larger diameter and a dendritic surface (Figure 2c,d). The thickness of the coating is ca. 400 nm (inset of Figure 2d). Energy-dispersive X-ray spectrometry (EDXS) characterization (Figure 2d,e) reveals the existence and homogeneous distribution of the Ni around the skeleton of the melamine foam, indicating that the Ni coating on the melamine foam has been well synthesized. Furthermore, it should be noted that the element P is also homogeneously distributed in the Ni layer (Figure 2f), which is believed to come from sodium hypophosphite during the process of reduction. To determine the chemical state of P in Ni, X-ray powder-diffraction (XRD) and X-ray photoelectron spectroscopy (XPS) of 3DDC were employed. As shown in Figure S1 (Supporting Information), the diffraction peaks could be indexed to metal Ni (JCPDS card, No. 04–0850), indicating that P is doped into Ni,[9,10] which is consistent with the XPS results (Figure S2, Supporting Information). To further verify the structure of the as-obtained Ni coating, transmission electron microscopy (TEM) was employed. The dendritic structure of the Ni coating with a diameter of ca. 200 nm can be seen in Figure 2g; it is crucial to the preparation of a binder-free electrode and improvement of electrochemical performance as discussed below. From Figure 2h it can be seen that the lattice spacing of the P-Ni coating is ca. 0.2 nm, which corresponds to the spacing of the (111) crystal face of metal nickel as shown in Figure S1. It should be noted that P-doped Ni coating could exhibit much-improved corrosion resistance,[11] which would benefit the stability of the current collector and its practical use in commercial LIBs, where the presence of very corrosive HF in the electrolyte cannot be excluded (see below).

The excellent mechanical stability of the current collector is crucial to its application in energy storage devices. As shown in **Figure 3**a, the 3DDC can bear a compression to 50% volume reduction and recover its original volume after release of the compression, indicating 3DDC is elastic and demonstrating a mechanically robust behavior.[12] Importantly, the excellent flexibility of 3DDC is maintained even after 600 cycles of compression testing and no obvious structural damage can be found, as shown in Figure S3 (Supporting Information). In sharp contrast, such favorable high flexibility cannot be achieved by previously reported commercial 3D metal materials (e.g., Ni foam, Cu foam, and Ti foam). In addition, the 3DDC shows good bending properties (Figure S4, Supporting Information). Furthermore, the electrical conductivity of our prepared lightweight and robust 3DDC reaches a very high value of up to 4800 S m^{-1}, which is much higher than that of most reported lightweight and flexible 3D conducting materials, including 3D graphene foam, carbon nanotube (CNT) conductive textiles, CNT aerogels, and Ag nanowire/polyurethane foam composites (Figure 3b).[13] Furthermore, the density of 3DDC with Ni-P coating is as low as ca. 29 mg cm^{-3}, which is far lower than that of other highly conductive 3D metal materials, including Ni nanofoams, porous Au, and Ti foam (Figure 3c).[14] As the current collector accounts for ca. 10% of the whole weight of current commercial LIBs, this very low density will help to increase the specific energy density of next-generation energy storage devices.[15] Furthermore, an organic solvent such as *N*-methyl pyrrolidone (NMP) is necessary in preparing

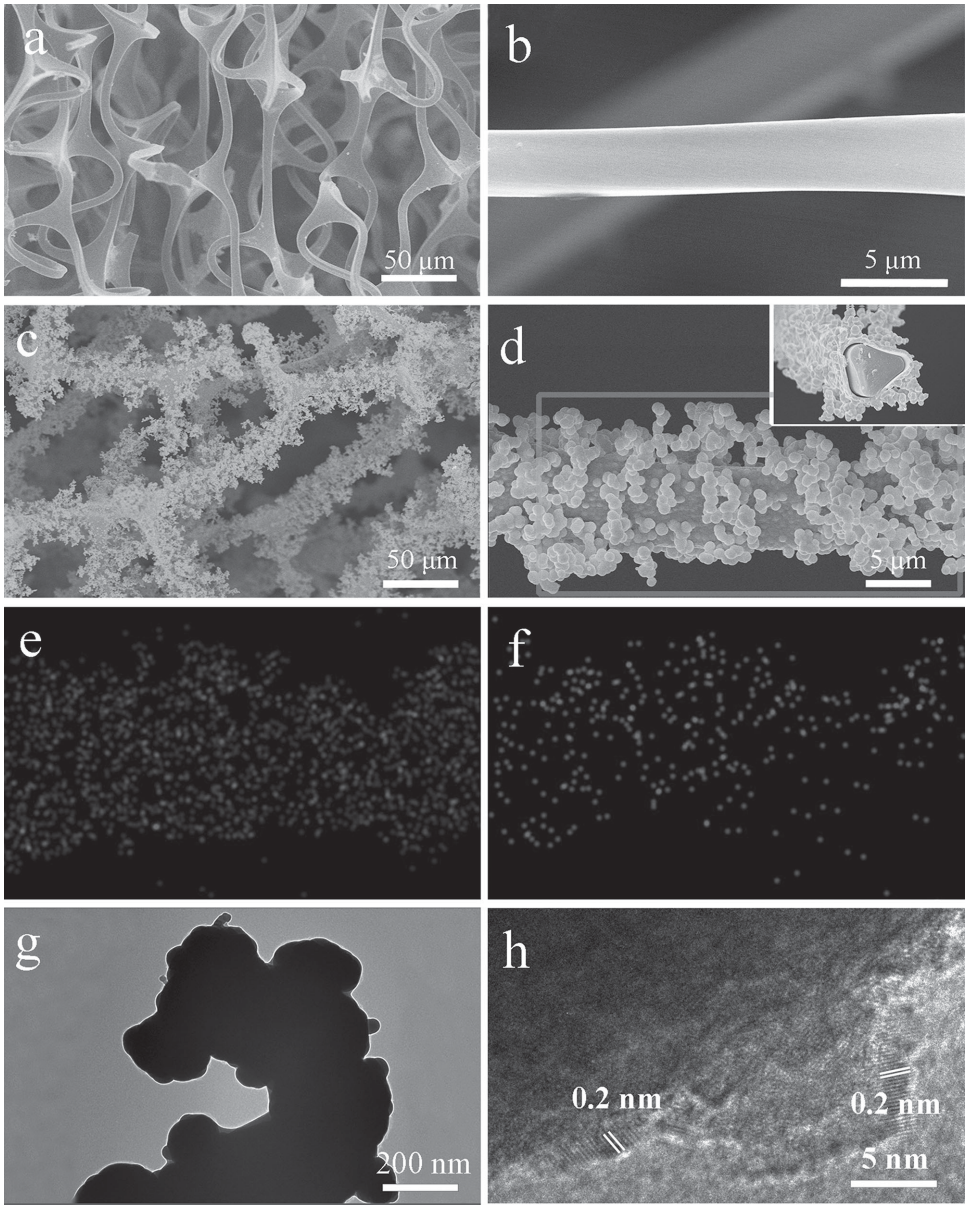

Figure 2. a,b) Low and high magnification SEM images of melamine foam. c,d) Low and high magnification SEM images of 3DDC. Inset: SEM image of cross-section of 3DDC. e,f) Elemental mapping images of nickel (e) and phosphorus (f) in the selected area (rectangle in (d)). g,h) Low- and high-magnification TEM images of dendritic Ni-P.

commercial electrodes to disperse the electrode materials and polymeric binder. However, the use of poisonous NMP inevitably pollutes the environment and increases the cost. On the other hand, because of its lower production cost and environmentally friendly nature, the preparation of electrodes using aqueous solutions is highly desirable, though still very challenging as most commercial current collectors are hydrophobic. Unexpectedly, as shown in Figures 3d–f, the 3DDC is superhydrophilic, while the commercial Ni foam is not (the water contact angle is ca. 87.5°). Additionally, the 3DDC and Ni foam are also organophilic, as shown in Figures 3g–i. The results show that the obtained 3DDC is amphipathic and thus both aqueous and organic solutions can be used to prepare electrodes.

The electrochemical stability of the current collector is crucial for applications in batteries. To verify the electrochemical stability of the 3DDC, cyclic voltammetry (CV) was performed. As shown in **Figure 4**a, it is found that our 3DDC is very stable even under a high potential, which is very similar to stable Al foil in the voltage range from 1.5 to 5 V. In sharp contrast, commercial Ni foam is unstable and exhibits obvious oxidation reaction at voltages beyond 3.6 V. To further evaluate the chemical stability of the 3DDC in the real electrolyte of LIBs, inductively coupled plasma atomic emission spectroscopy (ICP-AES) measurements were performed; only ca. 0.07 wt% Ni from the 3DDC was dissolved into the electrolyte after two weeks. In contrast, it was found that ca. 8.3 wt% Al from commercial Al

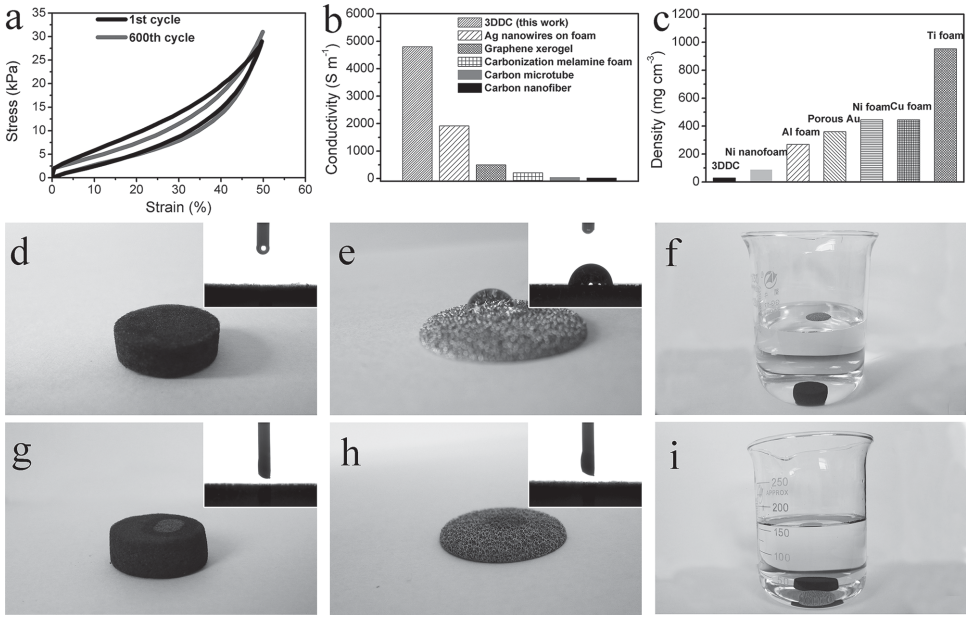

Figure 3. a) Loading and unloading compressive stress–strain curves of the 3DDC over 600 cycles. b) The electric conductivity of the 3DDC and reported robust materials. c) The density of the 3DDC and reported 3D metal materials. d,e) Photographs of water droplets on the surface of the 3DDC (d) and Ni foam (e). (f) Photograph of the 3DDC and Ni foam in water. g,h) Photographs of NMP droplets on the surface of the 3DDC (g) and Ni foam (h). i) Photograph of the 3DDC and Ni foam in NMP. Insets: Water and NMP contact angles for the 3DDC and Ni foam.

foil is dissolved into the electrolyte under the same conditions. The results demonstrate that our 3DDC is more favorable as a current collector in LIBs. The cycling stability of the current collector is very critical for application in LIBs. As shown in Figure 4b, the 3DDC is stable in the voltage range from 0 to 3 V even after 300 cycles, indicating that the -prepared 3DDC can be applied as the anode current collector. Importantly, the 3DDC is also stable in the voltage range from 1.5 to 5 V even after 300 cycles, and no obvious oxidation reaction can be found in Figure 4c. However, Ni foam exhibits a serious oxidation reaction due to decomposition of the over 6 cycles in the voltage range 1.5–5 V. The results demonstrate that our 3DDC can be used for the anode/cathode current collector in a wide voltage window (0–5 V).

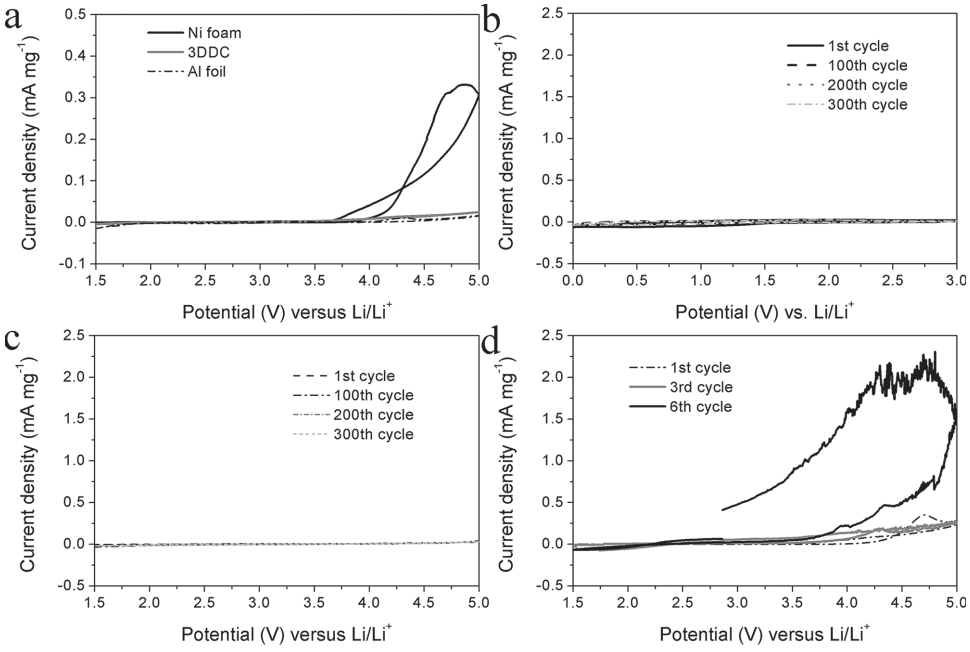

Figure 4. a) Cyclic voltammograms of the 3DDC, Ni foam, and Al foil at a scan rate of 1 mV s^{-1} in the voltage range 1.5–5 V for the first cycle. b) The electrochemical stability of the 3DDC at a scan rate of 1 mV s^{-1} in the voltage range 0–3 V. c,d) The electrochemical stability of the 3DDC (c) and Ni foam (d) at a scan rate of 1 mV s^{-1} in the voltage range 1.5–5 V.

Inspired by above confirmed advantages of our 3DDC, we then tested its efficacy as a novel current collector for the fabrication of a binder-free electrode. As a proof-of-concept application, germanium oxide (GeO_2) was intentionally chosen as a representative electrode material because it suffers from very low electrical conductivity and huge volume variation upon lithium insertion/extraction, which is a great challenge for a conventional current collector, to say nothing of a binder-free electrode. In a typical synthesis of a binder-free electrode with the 3DDC, GeO_2 (JCPDS card, No. 43–1016) was first dissolved in ammonia aqueous solution and then simply coated on the 3DDC by means of a facile dip-coating method (Figures S6,S7 in the Supporting Information). Especially, the mass loading of GeO_2 could be easily controlled by changing cycles of dip coatings. The morphology and structure of the as-prepared 3DDC/GeO_2 binder-free electrode was investigated by SEM and EDXS mapping technique (**Figure 5**a, Figure S7). It was found that the 3DDC/GeO_2 binder-free electrode has a porous morphology (Figure 5a), and the elements Ge and Ni are distributed homogeneously (Figure S7), demonstrating that the coating of GeO_2 around the skeleton of 3DDC is uniform and complete. It should be noted that, even without the help of polymer binder, no detachment of active materials from the 3DDC can be observed. The low-cost, scalable fabrication of the 3DDC/GeO_2 binder-free electrode was attributed to the amphipathic and dendritic nature of 3DDC, whereby the former property could help the adhesion of GeO_2 to the 3DDC in the aqueous solution during the preparation process, while the latter could help to anchor and confine the in situ growth of GeO_2. This binder-free and unique configuration will improve the electrochemical performance (see below). For comparison, electrodes of GeO_2 were prepared on commercial 3D Ni foam both without (GeO_2/Ni foam) and with the widely used water-soluble carboxymethyl cellulose (CMC) binder (GeO_2-CMC/Ni foam). In contrast to the 3DDC/GeO_2 electrode, even with the powerful CMC binder, the GeO_2 was found to detach easily from the Ni foam (Figure 5b,c), which leads to inferior electrochemical performance (see below) and further confirms the efficacy of our 3DDC. The schematic diagram in Figure S8 (Supporting Information) shows the merits of the 3DDC compared to commercial Ni foam. Because of the dendritic structure of the metal Ni, it is difficult to peel GeO_2 off of the 3DDC because of anchoring of the dendritic structure, as shown in Figures S7a and S8a. However, GeO_2 is easily detached from Ni foam because of its smooth large-scale surface and hydrophobic nature (Figure S8b,c).

Coin cells with metallic Li counter electrode were then assembled and the galvanostatic discharge/charge technique was employed to evaluate the electrochemical performance of all the above fabricated electrodes in the voltage window 0.01–1.5 V vs. Li/Li^+. As shown in Figure 5d,e, the initial discharge capacities of 3DDC/GeO_2 and binder-containing conventional electrodes (GeO_2-PVDF, where PVDF is poly(vinylidene difluoride)) are 2493 and 1847 mA h g^{-1}, respectively, and the reversible capacities are 1174 and 667 mA h g^{-1}, respectively, based on the whole weight of the active materials. The observed high initial capacities are probably attributable to the formation of a solid-electrolyte-interface (SEI) layer on the surface of the electrode owing to irreversible degradation of electrolyte,[16] which is in accordance with the CV analysis (Figure S9,

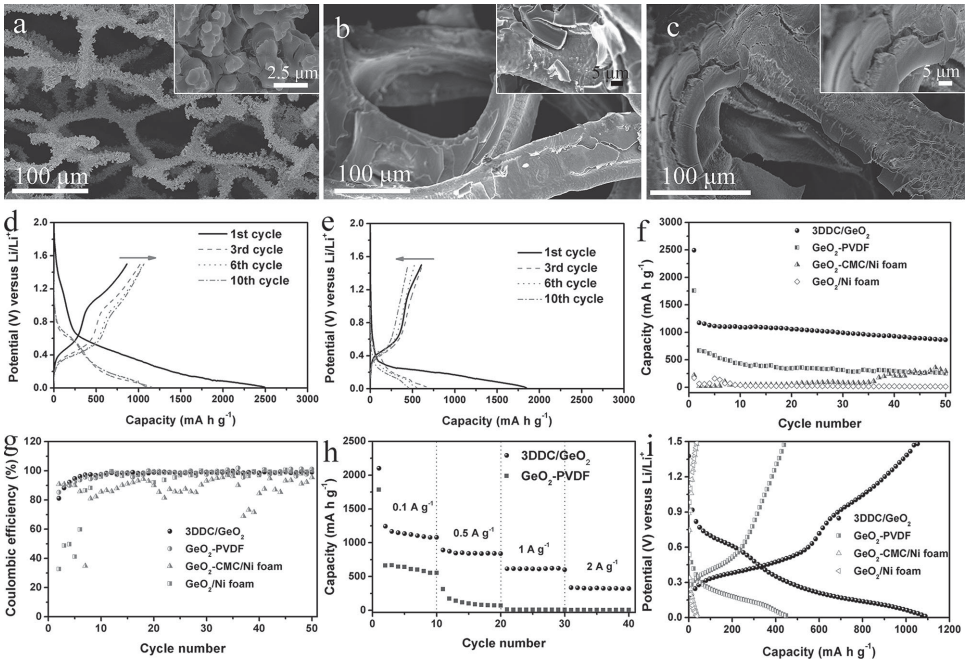

Figure 5. a–c) SEM images of 3DDC/GeO_2 (a), GeO_2/Ni foam (b), and GeO_2/Ni foam with binder (c). Insets: High magnification SEM images. d,e) Galvanostatic discharge/charge profiles of 3DDC/GeO_2 (d) and GeO_2 with binder (e) during the first ten cycles. f) Reversible Li extraction capacity of 3DDC/GeO_2, GeO_2 with binder, GeO_2/ Ni foam with binder, and GeO_2/Ni foam at 0.1 A g^{-1}. g) The coulombic efficiency of 3DDC/GeO_2, GeO_2 with binder, GeO_2/Ni foam with binder, and GeO_2/Ni foam at a current density of 0.1 A g^{-1}. h) Rate-capability performance of 3DDC/GeO_2 and GeO_2 with binder. i) Galvanostatic discharge/charge profiles of 3DDC/GeO_2, GeO_2 with binder, GeO_2/Ni foam with binder, and GeO_2/Ni foam at the tenth cycle.

Supporting Information). Note that the initial coulombic efficiency of the two electrodes is very low due to the formation of the SEI layer and the intrinsic properties of GeO_2, which is consistent with results reported for GeO_2.[17] It should be noted that the coulombic efficiency can be improved by adding extra sacrificial lithium or using a prelithiated electrode.[18] Interestingly, the charge–voltage plateau of 3DDC/GeO_2 declines gradually over the first six cycles, indicating the activation of the active materials. However, the charge–voltage plateau of the GeO_2-PVDF electrode does not stabilize for nine cycles. The results show that our 3DDC can improve the activation of the electrode. It should be noted that the SEI is robust and stable in the following cycles, as shown by the high coulombic efficiency (near to unity) compared to that of the GeO_2-PVDF electrode (Figure 5g). Additionally, it was found that our 3DDC/GeO_2 electrode exhibited much higher reversible capacity and more-stable cycling performance. Figure S10 (Supporting Information) shows the Nyquist plots of 3DDC/GeO_2 during the cycling process. The impedance of 3DDC/GeO_2 is very stable after two cycles, indicating a more stable electrode under cycling. The results further demonstrate that for 3DDC/GeO_2 it is necessary to cycle a number of times to activate the electrode. Note that the first charge-transfer resistance (R_{ct}) of the electrode is highest, owing to the formation of the SEI. And the decreasing impedance after subsequent cycles demonstrates an activation of the electrode. Figure 5f shows the cycling performance of four electrodes; the reversible capacities of 3DDC/GeO_2 and GeO_2-PVDF are ca. 1174 and 667 mA h g^{-1}, respectively. Note that the 3DDC exhibits very low discharge capacity (Figure S11, Supporting Information) and the higher capacity of 3DDC/GeO_2 is mainly attributed to GeO_2 in the 3DDC electrode. After 50 cycles, the reversible capacity of 3DDC/GeO_2 is still as high as 863 mA h g^{-1}, which is ca. 74% capacity retention. In sharp contrast, the cycling performance of GeO_2-PVDF is extremely poor. The reversible capacity of the GeO_2 electrode decreases from 667 to only 252 mA h g^{-1}, which is ca. 34% capacity retention, indicating very poor cycling stability compared to 3DDC/GeO_2. For further comparison, the cycling capacities of GeO_2/Ni foam and GeO_2-CMC/Ni foam were also estimated. The first discharge capacities are ca. 171 and 219 mA h g^{-1}, which is much less than the capacity of 3DDC/GeO_2. Especially, the GeO_2/Ni foam exhibits poor cycling performance. After 50 cycles, the capacity is only ca. 13.9 mA h g^{-1}. However, the capacity of GeO_2-CMC/Ni foam first increases to ca. 358 mA h g^{-1} and then decreases to ca. 295 mA h g^{-1}. The coulombic efficiency of the two electrodes based on Ni foam is also very unstable under cycling, as shown in Figure 5g. The poor cycling-capacity performance of the electrodes is mainly attributed to detachment of active materials from the Ni foam (Figure 5b,c).

To confirm the structural stability of the 3DDC/GeO_2 electrode upon cycling, we investigated the morphology of the as-prepared binder-free electrode after 50 discharge/charge cycles. As shown in Figure S12 (Supporting Information), the 3D interconnected network and porosity of the current collector are maintained without obvious structural damage, demonstrating the stability of the 3DDC/GeO_2 electrode. The results indicate that our dendritic, higher conductivity, robust, and porous 3DDC can obviously improve the capacity and cycling stability of LIBs. The obtained higher reversible capacity and cycling stability of 3DDC/GeO_2 compared to the other three electrodes reflect the synergy of three characteristics of the 3DDC electrode: 1) Higher electronic conductivity, which is due to the 3DDC current collector with continuous electronic migration pathways. 2) Porous structure, which facilitates the penetration of electrolyte into 3DDC/GeO_2 and buffers volume changes of GeO_2 during cycling. 3) In situ growth of GeO_2 on 3DDC, which can enhance the mechanical contact of the active materials and the current collector due to their dendritic structure and intrinsic amphipathic properties. These merits can improve the utilization of active materials, and enhance the stability and conductivity of the electrode, thus increasing the reversible capacity and cycling stability of the electrode.

Also significantly enhanced is the rate capability of the 3DDC electrode compared with the counterparts on commercial Cu foil (GeO_2-PVDF). Figure 5h shows the rate-capability performance of 3DDC/GeO_2 and GeO_2-PVDF. The cells were measured between 0.01 and 1.5 V at current densities from 0.1 to 2.0 A g^{-1}. At moderate current densities of 0.5 and 1 A g^{-1}, the capacity of 3DDC/GeO_2 is ca. 840 and 620 mA h g^{-1}, respectively, which is higher than that of GeO_2-PVDF (the capacity is ca. 70–330 and 8 mA h g^{-1}, respectively). Unexpectedly, at a higher current density of 2 A g^{-1}, 3DDC/GeO_2 is still able to deliver a discharge capacity of ca. 330 mA h g^{-1}, which is much higher than that of GeO_2-PVDF (only ca. 5 mA h g^{-1}). The enhanced rate capability is mainly attributed to the particular structure of 3DDC, in which the porous and continuous conductive network structure can shorten Li ion and electron diffusion paths and achieve rapid Li ion and electron diffusion times. Figure 5i shows galvanostatic discharge/charge profiles of 3DDC/GeO_2 and GeO_2-PVDF at the tenth cycle, so that activation of the electrode has been completed, as discussed above. These discharge/charge profiles are similar to those reported for GeO_2.[17] It is found that the discharge capacity of the 3DDC electrode is higher than those of the other three electrodes. Especially, the average discharge voltage of 3DDC/GeO_2 is ca. 0.241 V, which is higher than those of GeO_2-PVDF (0.164 V), GeO_2-CMC/Ni foam (0.127 V), and GeO_2/Ni foam (0.079 V). The results demonstrate that the 3DDC could lead to improved energy efficiency of LIBs as a result of its higher ion/electron conductivity and more stable electrode structure.

In summary, we have designed and demonstrated a facile method to fabricate a lightweight, low-cost, and robust (mechanical and chemical/electrochemical) 3D porous dendritic current collector, which shows high electronic conductivity, plentiful interconnected ion/electron and mass transport pathways, and high electrochemical stability over a wide voltage range up to 5 V. Furthermore, the 3DDC is dendritic and amphipathic, which enables the easy fabrication of a robust, binder-free electrode. As a proof-of-concept application, a binder-free 3DDC/GeO_2 electrode has been successfully obtained that shows superior electrochemical performance even compared to binder-containing conventional electrodes in terms of high specific capacity, cycling stability, and rate capability. It may prove possible to extend the 3DDC-boosted advantages to other electrochemical storage/conversion systems in which fast ion/electron and mass transport and mechanical, chemical, and electrochemical robustness are required.

Supporting Information

Supporting Information is available from the Wiley Online Library or from the author.

Acknowledgements

X.-l.H., D.X., and S.Y. contributed equally to this work. This work is financially supported by the 100 Talents Programme of the Chinese Academy of Sciences, National Program on Key Basic Research Project of China (973 Program, grant no. 2012CB215500), the National Natural Science Foundation of China (grant nos. 21101147 and 21203176), and the China Postdoctoral Science Foundation (2014M134792).

Received: June 18, 2014
Revised: July 30, 2014
Published online: September 18, 2014

[1] a) J. B. Goodenough, Y. Kim, *Chem. Mater.* **2010**, *22*, 587; b) M. Armand, J. M. Tarascon, *Nature* **2008**, *451*, 652; c) I. E. Rauda, V. Augustyn, B. Dunn, S. H. Tolbert, *Acc. Chem. Res.* **2013**, *46*, 1113; d) J. Luo, W. Cui, P. He, Y. Xia, *Nat. Chem.* **2010**, *2*, 760; e) W. Li, Y. Yin, S. Xin, W. Song, Y. Guo, *Energy Environ. Sci.* **2012**, *5*, 8007.

[2] a) J. Jiang, Y. Li, J. Liu, X. Huang, C. Yuan, X. W. Lou, *Adv. Mater.* **2012**, *24*, 5166; b) L. Li, F. Meng, S. Jin, *Nano Lett.* **2012**, *12*, 6030; c) J. Wang, N. Du, H. Zhang, J. Yu, D. Yang, *J. Mater. Chem.* **2012**, *22*, 1511; d) Y. Yu, C. Yan, L. Gu, X. Lang, K. Tang, L. Zhang, Y. Hou, Z. Wang, M. W. Chen, O. G. Schmidt, J. Maier, *Adv. Energy Mater.* **2013**, *3*, 281; e) X. Huang, H. Yu, J. Chen, Z. Lu, R. Yazami, H. H. Hng, *Adv. Mater.* **2014**, *26*, 1296; f) J. Qian, Y. Chen, L. Wu, Y. Cao, X. Ai, H. Yang, *Chem. Commun.* **2012**, *48*, 7070.

[3] X. Huang, R. Wang, D. Xu, Z. Wang, H. Wang, J. Xu, Z. Wu, Q. Liu, Y. Zhang, X. Zhang, *Adv. Funct. Mater.* **2013**, *23*, 4345.

[4] a) S. W. Kim, J. H. Yun, B. Son, Y. Lee, K. M. Kim, Y. M. Lee, K. Y. Cho, *Adv. Mater.* **2014**, *26*, 2977; b) G. Kim, S. Jeong, J. Shin, J. Cho, H. Lee, *ACS Nano* **2014**, *8*, 1907; c) B. Liu, P. Soares, C. Checkles, Y. Zhao, G. Yu, *Nano Lett.* **2013**, *13*, 3414; d) S. Chabi, C. Peng, D. Hu, Y. Zhu, *Adv. Mater.* **2014**, *26*, 2440; e) S. R. Gowda, A. L. M. Reddy, M. M. Shaijumon, X. Zhan, L. Ci, P. M. Ajayan, *Nano Lett.* **2011**, *11*, 101; f) H. Guan, X. Wang, S. Chen, Y. Bando, D. Golberg, *Chem. Commun.* **2011**, *47*, 12098.

[5] a) H. Zhang, X. Yu, P. V. Braun, *Nat. Nanotechnol.* **2011**, *6*, 277; b) J. Kim, S. H. Kang, K. Zhu, J. Y. Kim, N. R. Neale, A. J. Frank, *Chem. Commun.* **2011**, *47*, 5214.

[6] X. Lang, A. Hirata, T. Fujita, M. Chen, *Nat. Nanotechnol.* **2011**, *6*, 232.

[7] Z. Chen, W. Ren, L. Gao, B. Liu, S. Pei, H. Cheng, *Nat. Mater.* **2011**, *10*, 424.

[8] a) B. Guo, X. Wang, P. F. Fulvio, M. Chi, S. M. Mahurin, X. Sun, S. Dai, *Adv. Mater.* **2011**, *23*, 4661; b) L. Qie, W. Chen, Z. Wang, Q. Shao, X. Li, L. Yuan, X. Hu, W. Zhang, Y. Huang, *Adv. Mater.* **2012**, *24*, 2047; c) L. Zhao, Y. Hu, H. Li, Z. Wang, L. Chen, *Adv. Mater.* **2011**, *23*, 1385.

[9] X. Zhou, Y. Shen, *J. Mater. Sci.* **2014**, *49*, 3755.

[10] S. Tian, J. Chen, *Fuel Process. Technol.* **2014**, *122*, 120.

[11] a) R. H. Guo, S. X. Jiang, Y. D. Zheng, J. W. Lan, *J. Appl. Polym. Sci.* **2013**, *127*, 4186; b) U. K. Fatema, Y. Gotoh, *J. Coat. Technol. Res.* **2013**, *10*, 415; c) J. Sudagar, J. Lian, W. Sha, *J. Alloys Compd.* **2013**, *571*, 183.

[12] M. Mecklenburg, A. Schuchardt, Y. K. Mishra, S. Kaps, R. Adelung, A. Lotnyk, L. Kienle, K. Schulte, *Adv. Mater.* **2012**, *24*, 3486.

[13] a) N. Li, Z. Chen, W. Ren, F. Li, H. Cheng, *Proc. Natl. Acad. Sci. USA*, **2012**, *109*, 17360; b) L. Hu, F. La Mantia, H. Wu, X. Xie, J. McDonough, M. Pasta, Y. Cui, *Adv. Energy Mater.* **2011**, *1*, 1012; c) Z. Wu, C. Li, H. Liang, J. Chen, S. Yu, *Angew. Chem. Int. Ed.* **2013**, *52*, 2925; d) J. Ge, H. Yao, X. Wang, Y. Ye, J. Wang, Z. Wu, J. Liu, F. Fan, H. Gao, C. Zhang, S. Yu, *Angew. Chem. Int. Ed.* **2013**, *52*, 1654.

[14] a) J. M. Haag, G. Pattanaik, M. F. Durstock, *Adv. Mater.* **2013**, *23*, 3238; b) J. Banhart, *Prog. Mater. Sci.* **2001**, *46*, 559; c) K. Zhang, X. Tan, J. Zhang, W. Wu, Y. Tang, *RSC Adv.* **2014**, *4*, 7196; d) J. Chen, K. Sheng, P. Luo, C. Li, G. Shi, *Adv. Mater.* **2012**, *24*, 4569; e) Y. Zhu, H. Hu, S. Sun, G. Ding, *Int. J. Refrig.* **2014**, *38*, 215; f) H. Hsu, S. Hsu, S. Wu, P. Wang, W. Ho, *J. Alloys Compd.* **2013**, *575*, 326.

[15] K. Richa, C. W. Babbitt, G. Gaustad, X. Wang, *Resour., Conserv. Recycl.* **2014**, *83*, 63.

[16] a) S. Brutti, V. Gentili, H. Menard, B. Scrosati, P. G. Bruce, *Adv. Energy Mater.* **2012**, *2*, 322; b) C. Peng, B. Chen, Y. Qin, S. Yang, C. Li, Y. Zuo, S. Liu, J. Yang, *ACS Nano* **2012**, *6*, 1074.

[17] a) B. Liu, A. Abouimrane, M. Balasubramanian, Y. Ren, K. Amine, *J. Phys. Chem. C* **2014**, *118*, 3960; b) D. T. Ngo, R. S. Kalubarme, M. G. Chourashiya, C. Park, C. Park, *Electrochim. Acta* **2014**, *116*, 203; c) D.-L. Ma, S. Yuan, X.-L. Huang, Z.-Y. Cao, *Energy Technol. (Weinheim, Ger.)* **2014**, *2*, 342.

[18] a) C. R. Jarvis, M. J. Lain, M. V. Yakovleva, Y. Gao, *J. Power Sources* **2006**, *162*, 800; b) N. Liu, L. Hu, M. T. McDowell, A. Jackson, Y. Cui, *ACS Nano* **2011**, *5*, 6487.